

'Checkerboard stripe' electronic state on cleaved surface of $\text{NdO}_{0.7}\text{F}_{0.3}\text{BiS}_2$ probed by scanning tunneling microscope

T. Machida¹, Y. Fujisawa¹, M. Nagao^{2,3}, S. Demura³, K. Deguchi³, Y. Mizuguchi⁴, Y. Takano³ and H. Sakata¹

¹*Department of Physics, Tokyo University of Science,
1-3 Kagurazaka, Shinjuku-ku, Tokyo 162-8601, Japan*

²*University of Yamanashi, 7 -32 Miyamae, Kofu 400-8511, Japan*

³*National Institute for Materials Science, 1-2-1 Sengen, Tsukuba, Ibaraki 305-0047, Japan*

⁴*Electrical and Electronic Engineering, Tokyo Metropolitan University,
1-1 Minami-osawa, Hachioji, Tokyo 192-0397, Japan*

(Dated: March 25, 2014)

We present scanning tunneling microscopy measurements on a cleaved surface of the recently discovered superconductor $\text{NdO}_{0.7}\text{F}_{0.3}\text{BiS}_2$ with the transition temperature (T_c) = 5.1 K. Tunneling spectra at 4.2 K (below T_c) and 22 K (above T_c) show a large spectroscopic gap (~ 40 mV), which is inconsistent with the metallic nature in the bulk measurements. Moreover, we find two interesting real-space electronic structures. First is a 'checkerboard strip' electronic state characterized by the alternating arrangement of two types of nano-clusters. In one cluster, one-dimensional electronic stripes run along one Bi-Bi direction, whereas, in the other cluster, the stripes do along the other Bi-Bi direction. Second is a nanoscale electronic inhomogeneity whose microscopic source seems to be atomic defects on the cleaved surface or dopant F atoms. We conclude that the observed electronic features are inherent in the cleaved surface.

For recent past decades, several layered compounds have generated much sustained interest, because of their peculiar phenomena. One example of these phenomena is charge-density-wave (CDW) in the transition metal dichalcogenides¹⁻⁷ and trichalcogenides^{8,9} in which the superconductivity (SC) often coexists with the CDW¹⁻⁷. Because of the coexistence of CDW and SC, these materials have been fascinating as an ideal stage for understanding the interplay between these phenomena^{4,5,7}. Another example is the high temperature superconductivity in the copper oxides¹⁰ and iron-pnictides¹¹. The superconductivity in these materials often coexists with or emerges in the proximity of some electronic ordered states¹²⁻¹⁸, which breaks C_4 -symmetry of the underlying crystal lattice. The explorations of the relation between SC and the electronic ordered states have offered intriguing information in understanding of the mechanisms of the unconventional superconductivity.

Recent discovery of the BiS_2 superconductors has triggered vigorous research activities, because of (i) the structural similarity with the cuprates and pnictides and (ii) their relatively high T_c ¹⁹⁻²⁷. Recent theoretical calculations have suggested that a quasi-one-dimensional character of the band dispersion provides a good Fermi surface nesting²⁸⁻³². Some of them have proposed that an unstable phonon at $\mathbf{q} = (\mathbf{q}, \mathbf{q}, 0)$ corresponding to Fermi surface nesting vector causes a CDW instability^{29,30}. It has been argued vigorously how the SC is related to this Fermi surface nesting²⁸⁻³⁵. Meanwhile, the symmetry of the superconducting gap has been also investigated theoretically and experimentally. These studies have suggested the isotropic s -, anisotropic s -, and d -wave symmetries as possible pairing symmetries^{33,36,37}. Despite these studies described above, there is less conclusive empirical evidence to determine the pairing symmetry and to uncover whether CDW instability occurs or not.

One of powerful technique to address directly these issues is scanning tunneling spectroscopy (STS) using scanning tunneling microscope (STM) which has determined the pairing symmetries in a large variety of the superconductors³⁸⁻⁴². Additionally, this technique has made a significant contribution not only to visualize the CDW^{3,6} and other electronic ordered states^{13,14,16,17} but also to disentangle the relation between the superconductivity and the electronic ordered states.

However, the results obtained by these surface sensitive probes occasionally do not reflect intrinsic bulk nature but do dominantly nature peculiar to the surface which is sometimes a stage of a novel phenomenon, when the structure and the electronic nature on the surface is different from those in the bulk. Hence, it is necessary to uncover what kind of surface structure and electronic states are realized on an exposed surface, as a first step for investigating the electronic nature in a new layered compounds.

In this paper, we performed STM and STS experiments on a cleaved surface of $\text{NdO}_{0.7}\text{F}_{0.3}\text{BiS}_2$ ($T_c \sim 5.1$ K) which is one of the BiS_2 superconductors. A typical STM image on a cleaved surface shows several features; (i) a square lattice with a period of ~ 3.9 Å corresponding to the in-plane lattice parameter, (ii) atomic defects, and (iii) a streaked depression which is centered on the atomic defect. The tunneling spectroscopy captures several unexpected phenomena. First is a large spectroscopic gap (~ 40 mV) without coherence peak, which survives well above T_c . Second is a square lattice characterized by the alternating arrangement of two types of nano-clusters. In one cluster, one-dimensional stripe electronic structures run along one of Bi-Bi direction, whereas, in the other cluster, the stripes run along the other Bi-Bi direction. Third is a nanoscale electronic inhomogeneity. By comparing these electronic features with the previous

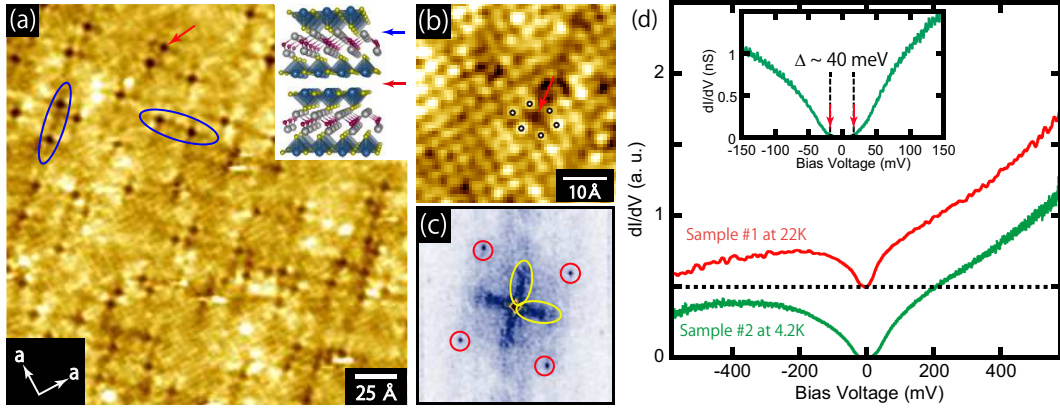


FIG. 1. (Color online) (a) A typical STM image on a $240 \times 240 \text{ Å}^2$ field of view taken at $V_s = +500 \text{ mV}$ and $I_{set} = 500 \text{ pA}$. Inset illustrates schematic figure of the crystal structure, where red, gray, yellow, blue spheres represent Nd, O, S, and Bi atoms, respectively. (b) A magnified STM image on a $45 \times 45 \text{ Å}^2$ field of view. (c) A Fourier transform image of (a). Red circles indicate the spots corresponding to the atomic array. Yellow ellipsoids mark the tails corresponding to the dark streaks running along the diagonal (110) direction of the unit cell. (d) Typical tunneling spectra taken at $V_s = +500 \text{ mV}$ and $I_s = 1.0 \text{ nA}$. Red (upper) and Green (lower) lines represents the spectra taken on the sample # 1 at 22 K and sample # 2 at 4.2 K. The red spectrum is shifted by 0.5 for clarity. The dashed line indicates the zero conductance for the red (shifted) spectrum. Inset shows the spectrum with higher energy resolution.

bulk measurements and theoretical calculations, the observed electronic features are believed to be inherent in the cleaved surface.

Single crystals used in this study were grown by a high-temperature flux method, detailed in elsewhere²⁵. The superconducting transition temperature of 5.1 K was determined by magnetization and resistivity measurements²⁵. A laboratory-made LT-STM was used for STM/STS measurements. The STS measurements were performed in a helium-gas environment at 4.2 K and 22 K on a surface that were prepared by cleaving the sample in situ in a pure helium gas. We measured the I - V characteristics and obtained the tunneling spectra by numerical differentiation.

We display typical STM images in Fig. 1(a) and (b) indicating a square lattice with a period of $\sim 3.9 \text{ Å}$ corresponding to the in-plane lattice parameter. This is confirmed from four spots in FT image marked by red circles in Fig. 1(c). In addition to the square lattice, several dark spots can be observed. In STM measurements on the layered compounds, it is quite important to identify which plane appears as an exposed surface. In this material, there are three possible atomic planes which could be exposed; (i) NdO, (ii) S(2), and (iii) BiS(1) planes. If the cleavage occurs between NdO and S(2) layers as shown by a blue arrow in the inset of Fig. 1(a), two types of the surfaces [NdO and S(2) planes] should be exposed. On the other hand, if the cleavage occurs between two BiS(1) layers shown by a red arrow in the inset, only one type of the surface [BiS(1) plane] should be exposed. Because we obtained only one type of the STM images as shown in Fig. 1(a) and the tunneling spectrum in Fig. 1(d) in this study, we conclude that the observed surface is BiS(1) plane. Recent density of states calculations³¹ assert that

the Bi- p and S(1)- p states dominantly contribute to the density-of-states and that the Bi- p DOS is higher than that of S(1)- p near E_F . Therefore, the observed bright spots in the STM images are believed to be the Bi atoms.

Given that the observed bright spots are the Bi atoms, the observed dark spots as pointed by the red arrow in Fig. 1(a) and (b) are Bi defects, since the center of the dark spot coincides with one of the four Bi sites of the Bi square lattice as shown in Fig. 1(b). The density of the dark spots is about 3% per Bi atom, which is consistent with the results of the recent single crystal X-ray diffraction measurements⁴³. Besides the atomic defects, the slightly dark streaks run along approximately diagonal directions of the unit cell. The representative examples are marked by two blue ellipsoids in Fig. 1(a). The direction and the length of the dark streaks show somewhat variability. This variability corresponds to the four tails extending from the center ($\mathbf{q} = 0$) in the FT image as marked by yellow ellipsoids in Fig. 1(c). It appears that the dark streaks are highly related to the atomic defects. Therefore, the dark streaks seem to be derived from the structural distortion relaxing the mechanical stress due to the atomic defects.

Figure 1(d) shows typical tunnelling spectra at 4.2 and 22 K (different samples and different tips). Both spectra indicate (i) a large energy asymmetry characterized by the higher conductance in positive energy than that in negative, and (ii) a spectroscopic gap characterized by a depression of the spectral weight around E_F . Surprisingly, there is less state between $\pm 20 \text{ meV}$ at both 4.2 and 22 K. Because of the lack of the coherence peak and of gap existence well above T_c , it is thought that the observed gap is not superconducting gap. These spectroscopic features are not consistent with the bulk prop-

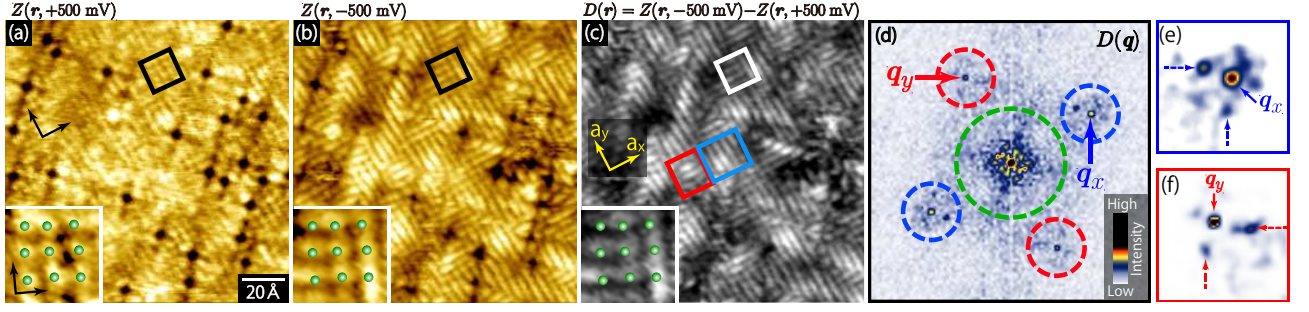


FIG. 2. (Color online) (a) and (b) STM images on a $130 \times 130 \text{ \AA}^2$ FOV taken at $V_s = +500$ and -500 mV. (c) Difference between (a) and (b) ($D(\mathbf{r})$ -map) ; $D(\mathbf{r}) = Z(\mathbf{r}, -500 \text{ mV}) - Z(\mathbf{r}, +500 \text{ mV})$. Red and blue boxes indicate the representatives of the unidirectional nano-domains where the streak structures runs along a_x and a_y directions, respectively. Insets of (a), (b), and (c) are magnified images in the FOV marked by black and white boxes in (a) to (c), respectively. These magnified images are rotated by 40° in a clockwise fashion. Green spheres represents Bi atom sites. (d) Fourier transform image [$D(\mathbf{q})$] of (c). Red and blue dashed circles indicate the size of Λ (cutoff frequency) in the inverse FT analyses for the stripe structures. Green dashed circle indicate the size of Λ for inhomogeneous structure. (e) and (f) magnified image of (d) around \mathbf{q}_x and \mathbf{q}_y . Here, we increase the contrasts in these magnified image for clarity. Dashed arrows in these images indicate satellite peaks.

erties showing the clear superconducting transition and the metallic behavior of the resistivity just above T_c ²⁵. Therefore, it is preferable to consider that the observed spectroscopic features do not reflect the bulk property but do the property peculiar to the surface.

To explore the spatial variation of the electronic structure, we compare two STM images taken at $V_s = +500$ and -500 mV on the same FOV as shown in Figs. 2(a) [$Z(\mathbf{r}, +500 \text{ mV})$] and (b) [$Z(\mathbf{r}, -500 \text{ mV})$]. Apparently, there are two features which are more pronounced in the image at $V_s = -500$ mV than at $+500$ mV; (i) Fine stripe structures along the two a -axes and (ii) inhomogeneous contrasts on the background. We take the difference of these images [$D(\mathbf{r}) = Z(\mathbf{r}, -500 \text{ mV}) - Z(\mathbf{r}, +500 \text{ mV})$], as shown in Fig. 2(c). This process cancels the geometric information and extracts the electronic structures. In this case, the $D(\mathbf{r})$ -map indicates an energy asymmetry of the energy-integrated LDOS from 0 to ± 500 meV. The two features in $Z(\mathbf{r}, -500 \text{ mV})$ map are emphasized in $D(\mathbf{r})$ -map. Therefore, these two features are derived from the electronic spatial variation not geometric. The FT image of $D(\mathbf{r})$ -map in Fig. 2(d) ensure the existence of these two electronic features. The four spots marked by red and blue dashed circles correspond to the fine stripe structures, whereas the broad structure around $\mathbf{q} = 0$ marked by a green dashed circle does the inhomogeneous structure.

First, we focus on the fine stripe structures being elongated along one Bi-Bi direction. As described above, the stripe structures can be classified into two types. One modulates along a_x direction marked by a blue box in Fig. 2(c), (x -modulation) whereas the other does along a_y direction shown by a red box (y -modulation). These modulations form two types of nano-scale clusters: In one cluster, x -modulation predominates, whereas, in the other, y -modulation does. The FT image of $D(\mathbf{r})$ -map corroborates the presence of two modulations with the

period of a_0 , as shown in Fig. 2(d). Here we name the \mathbf{q} vectors corresponding to these two modulations as \mathbf{q}_x and \mathbf{q}_y , respectively. Moreover, it appears that the two type of clusters tend to be aligned alternately and periodically in Fig. 2(c). In FT image, besides the peaks at \mathbf{q}_x and \mathbf{q}_y , two satellite peaks can be seen around \mathbf{q}_x and \mathbf{q}_y as shown by dashed arrows in Figs. 2(e) and (f) (\mathbf{q}_{st}). These satellites indicate that the amplitudes of the observed x - and y -modulations periodically and two-dimensionally vary in real-space: these satellites are indicative of the alternating arrangement of the observed two types of clusters. The period of the amplitude modulations can be estimated from $\delta\mathbf{q} = \mathbf{q}_x \text{ or } \mathbf{q}_y - \mathbf{q}_{st}$. The $\delta\mathbf{q}$ is approximately $0.185 \times 2\pi/a_0$ ($0.245 \times 2\pi/(\sqrt{2}a_0)$). This means that the period of the amplitude modulation is approximately $5.4a_0$ ($4.1\tilde{a}_0$, \tilde{a}_0 is the length between Bi atoms along diagonal direction of the unit cell).

To visualize the corrugation of these clusters more clearly, we extract the components associated with the x - and y -modulations from the $D(\mathbf{r})$ -map using the inverse Fourier transformation as follows:

$$D(\mathbf{q}_\mu, \mathbf{r}) = \frac{2\pi}{N} \sum_{\mathbf{q}} D(\mathbf{q}) \exp(-i\mathbf{q} \cdot \mathbf{r}) \exp[-(\mathbf{q}_\mu - \mathbf{q})^2/\Lambda^2], \quad \mu = x \text{ or } y, \quad (1)$$

where Λ is a cut off frequency. Here we set the $\Lambda = 0.294 \times 2\pi/a_0$ ($1/\Lambda = 13.5 \text{ \AA}$) corresponding to the red and blue dashed circles in Fig. 2(d), as the Λ contains the satellite peaks. Figures 3(a) and (b) are the real parts of $D(\mathbf{q}_x, \mathbf{r})$ and $D(\mathbf{q}_y, \mathbf{r})$, respectively. A region with a large amplitude of the x -modulation shows a small amplitude of the y -modulation and vice versa. This is also confirmed more clearly in Fig. 3(c) in which Fig. 3(a) is superimposed on Fig. 3(b). Thus, our results suggest that the observed nano-clusters form a 'checkerboard' like

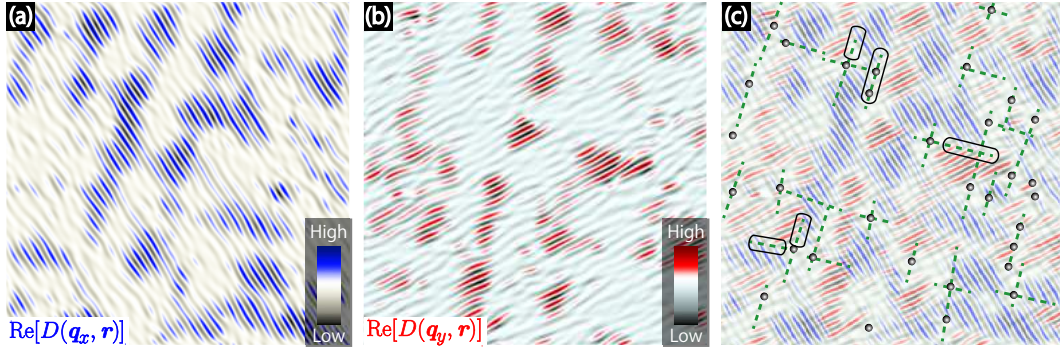


FIG. 3. (Color online) (a) and (b) Inverse FT images obtained by Fourier filtering out all the modulations except those surrounding q_x (a) and q_y (b), respectively: Images of the real part of $D(q_x, \mathbf{r})$ and $D(q_y, \mathbf{r})$, as shown in Eq. (1). (c) Superposition of (a) and (b). Black dots and green dashed lines correspond to the atomic defects and the dark streaks on the surface. Black boxes mark the dark streaks which are coincides with the boundary between two nano-clusters.

$4\tilde{a}_0$ square lattice. The formation of the lattice implies that some interactions exist between the nano-clusters.

Figure 3(c) shows the spatial correlation among the atomic defects, the dark streak structures and the observed nano-clusters. There is a slight correlation between the atomic defects and the stripe structures in these nano-clusters. The stripe structure tends to be suppressed around the atomic defects. The positions of the dark streak structures sometimes coincide with a boundary between two nano-clusters, as marked by the black boxes in Fig. 3(c). This means that the dark streak structure tends to pin the boundary of these clusters. Thus, these local perturbations seem to cause the distortion of the near $4\tilde{a}_0$ square lattice.

The observed electronic features including a large spectroscopic gap and 'checkerboard stripe' electronic structure have not been anticipated in the previous works which have investigated the bulk properties. Additionally, the 'checkerboard stripe' electronic structure is sensitive to the surface defects (atomic defects and dark streak structure). Therefore, it is conceivable that these electronic features appear to be inherent phenomena on the cleaved surface rather than the bulk.

In discussing why do the observed nano-clusters with the one-dimensional stripe appear on the cleaved surface, it is a key ingredient what breaks C_4 -symmetry. One possible candidate is the softening of the phonon. Recent calculation of the phonon spectra for $\text{LaO}_{1-x}\text{F}_x\text{BiS}_2$ predicted that it can occur that S(1) atoms move towards Bi atoms along the a -axis (or b -axis) due to the unstable phonon around Γ in the proper conditions³⁰. If this distortion occurs, the unit cell no longer maintains tetragonal symmetry (C_4 -symmetry) and the cell has orthogonal symmetry. Thus, it seems to be able to explain the unidirectional nature observed in this study. However, even if we adopt this idea, several questions still remain. Why do the nano-clusters form the near $4\tilde{a}_0$ square lattice? Whether the condition of the exposed surface obtained by cleaving the sample is proper to induce such unsta-

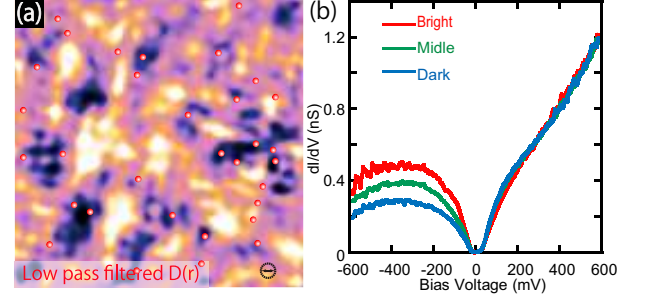


FIG. 4. (Color online) (a) Low pass filtered image of Fig. 1(c). In this low pass filtering process, we set the cutoff frequency to be $|\mathbf{q}| = 0.58 \times 2\pi/a_0$ corresponding to the real-space cutoff radius of 6.7 \AA indicated by a black circle on the bottom-right corner. Red dots show the positions of the atomic defects. (b) Tunneling spectra at several locations. Red, green, and blue lines indicate the spectrum taken at the bright, medium contrast, dark region in (a).

ble phonon, or not? Thus, a clear origin of the observed 'checkerboard strip' electronic structure remains an open question.

Next, we focus on the inhomogeneous structures. Figure 4(a) shows a low pass filtered image of $D(\mathbf{r})$ -map, where the cutoff frequency is $q_{\text{cut}} = 0.58 \times 2\pi/a_0$ (corresponding to the cutoff radius $r_{\text{cut}} = 6.7 \text{ \AA}$). This filtering process subtracts the fine stripe structures and extracts the electronic inhomogeneity. This filtered image contains inhomogeneous spatial variations of the energy integrated LDOS in both the $Z(\mathbf{r}, -500 \text{ mV})$ and $Z(\mathbf{r}, +500 \text{ mV})$. In this case, however, the contribution from the $Z(\mathbf{r}, -500 \text{ mV})$ appears to be larger than that from $Z(\mathbf{r}, +500 \text{ mV})$, because there is a larger contrast regarding the inhomogeneous spatial variation in the $Z(\mathbf{r}, -500 \text{ mV})$ than that in $Z(\mathbf{r}, +500 \text{ mV})$ as shown in Figs. 2(a) and (b). Thus, the bright region in the filtered $D(\mathbf{r})$ -map seems to correspond to the region with larger energy inte-

grated DOS from 0 to -500 meV. To further explore how does the shape of the tunneling spectrum change along the observed inhomogeneity, we take tunneling spectra at several locations with the different intensities of $D(\mathbf{r})$, as shown in Fig. 4(b). Here, we set the set bias voltage V_s to be +500 mV, because the spatial variation of the energy-integrated DOS in $Z(\mathbf{r}, +500 \text{ mV})$ is smaller than that in $Z(\mathbf{r}, -500 \text{ mV})$. This set-up condition appears to alleviate a set point effect on the tunneling spectrum. An apparent change in the spectral weight lies below -100 meV. Thus, the LDOS below -100 meV is highly sensitive to a source of the inhomogeneity.

The observed inhomogeneity is slightly correlated with the atomic defects: the defects prefer to sit on the dark region with the lower DOS in negative energy. This slight correlation implies that the atomic defects can be one of the possible sources of the electronic inhomogeneity. The inhomogeneous distribution of the dopant F atoms can also be the source of the inhomogeneity, because dopant atoms usually distribute in a random fashion. These local perturbations provide several causes inducing the electronic inhomogeneity. The representative causes are believed to be (i) a local strain leading to the local modification of the hopping integrals and (ii) an inhomogeneous distribution of the carrier density introduced by the dopants (F atoms).

In this paper, we report on STM and STS experiments on a cleaved surface of $\text{NdO}_{0.7}\text{F}_{0.3}\text{BiS}_2$ with $T_c = 5.1 \text{ K}$. The STM images contain the square lattice with the period of $\sim 3.9 \text{ \AA}$ corresponding to the lattice parameter along the a -axis and the several atomic defects. The tunneling spectra indicate the large spectroscopic gap ($\sim 40 \text{ mV}$) which is not the superconducting gap. In addition to this spectroscopic gap, we find two unexpected electronic structures; (i) 'checkerboard stripe' electronic structure and (ii) nanoscale electronic inhomogeneity. The former is characterized by the alternating arrangement of two types of clusters. In one cluster, one-dimensional stripe structures run along one of the crystal a -axes with a period of a_0 . In the other cluster, the stripes run along the other a -axis. Furthermore, these clusters form a square lattice with a period of near $4\tilde{a}_0$ along the diagonal directions of the unit cell. The latter seems to be related to the inhomogeneous distributions of the atomic defects and of the doped F atoms. By comparing our results with the previous bulk measurements, we conclude that the observed electronic features are inherent in the cleaved surface. These findings should be taken into account in discussing the electronic nature in this material by using results from surface sensitive probes such as ARPES and tunneling measurements.

-
- ¹ D. E. Moncton, J. D. Axe, and F. J. DiSalvo, Phys. Rev. B **16**, 891 (1977).
 - ² M. Naito, and S. Tanaka, J. Phys. Soc. Jpn. **51**, 219 (1982).
 - ³ A. Soumyanarayanan *et al.*, Proc. Natl. Acad. Sci. **110**, 1623 (2013).
 - ⁴ B. Sipos *et al.*, Nature Material **7**, 960 (2008).
 - ⁵ L. J. Li *et al.*, Euro. Phys. Lett. **97**, 67005 (2012).
 - ⁶ J.-J. Kim, W. Yamaguchi, T. Hasegawa, and K. Kitazawa, Phys. Rev. Lett. **73**, 2103 (1994).
 - ⁷ R. Ang *et al.*, Phys. Rev. Lett. **109**, 176403 (2012).
 - ⁸ N. Ru *et al.*, Phys. Rev. B **77**, 035114 (2008).
 - ⁹ H. J. Kim, *et al.*, Phys. Rev. Lett. **96**, 226401 (2006).
 - ¹⁰ J. G. Bednorz and K. A. Muller, Z. Phys. B: Condens. Matter **64**, 189 (1986).
 - ¹¹ Y. Kamihara, T. Watanabe, M. Hirano, and H. Hosono, J. Am. Chem. Soc. **130**, 3296 (2008).
 - ¹² S. A. Kivelson *et al.*, Rev. Mod. Phys. **75**, 1201 (2003).
 - ¹³ C. V. Parker *et al.*, Nature **468**, 677 (2010).
 - ¹⁴ M. J. Lawler *et al.*, Nature (London) **466**, 347 (2010).
 - ¹⁵ A. Mesaros *et al.*, Science **333**, 426 (2011).
 - ¹⁶ Y. Kohsaka *et al.*, Nature Physics **8**, 534 (2012).
 - ¹⁷ T.-M. Chuang *et al.*, Science **327**, 181 (2010).
 - ¹⁸ S. Kasahara *et al.*, Nature **486**, 382 (2012).
 - ¹⁹ Y. Mizuguchi *et al.*, Phys. Rev. B **86**, 220510(R) (2012).
 - ²⁰ S. K. Singh *et al.*, J. Am. Chem. Soc. **134**, 16504 (2012).
 - ²¹ Y. Mizuguchi *et al.*, J. Phys. Soc. Jpn. **81**, 114725 (2012).
 - ²² J. Xing, S. Li, X. Ding, H. Yang, and H.-H. Wen, Phys. Rev. B **86**, 214518 (2012).
 - ²³ R. Jha, A. Kumar, S. K. Singh, V.P.S. Awana, J. Supercond. Nov. Magn. **26**, 499 (2013).
 - ²⁴ S. Demura *et al.*, J. Phys. Soc. Jpn. **82**, 033708 (2013).
 - ²⁵ M. Nagao *et al.*, J. Phys. Soc. Jpn. **82**, 113701 (2013).
 - ²⁶ X. Lin *et al.*, Phys. Rev. B **87**, 020504(R) (2013).
 - ²⁷ D. Yazici *et al.*, Phys. Rev. B **87**, 174512 (2013).
 - ²⁸ H. Usui, K. Suzuki, and K. Kuroki, Phys. Rev. B **86**, 220501(R) (2012).
 - ²⁹ X. Wan, H.-C. Ding, S. Y. Savrasov, and C.-G. Duan, Phys. Rev. B **87**, 115124 (2013).
 - ³⁰ T. Yildirim, Phys. Rev. B **87**, 020506(R) (2013).
 - ³¹ B. Li, Z. W. Xing and G. Q. Huang, Euro. Phys. Lett. **110**, 47002 (2013).
 - ³² G. B. Martins, A. Moreo, and E. Dagotto, Phys. Rev. B **87**, 081102(R) (2013).
 - ³³ Y. Gao, arXiv:1304.2102 (2013).
 - ³⁴ Y. Yang, W.-S. Wang, Y.-Y. Xiang, Z.-Z. Li, and Q.-H. Wang, Phys. Rev. B **88**, 094519 (2013).
 - ³⁵ J. Lee *et al.*, Phys. Rev. B **87**, 205134 (2013).
 - ³⁶ Shruti, P. Srivastava and S. Patnaik, J. Phys.: Condens. Matter **25**, 312202 (2013).
 - ³⁷ G. Lamura *et al.*, Phys. Rev. B **88**, 180509(R) (2013).
 - ³⁸ Ø. Fischer, M. Kugler, I. Maggio-Aprile, and C. Berthod, Rev. Mod. Phys. **79**, 353 (2007).
 - ³⁹ J. E. Hoffman, Rep. Prog. Phys. **74**, 124513 (2011).
 - ⁴⁰ K. McElroy *et al.*, Nature (London) **422**, 592 (2003).
 - ⁴¹ T. Hanaguri, S. Niitaka, K. Kuroki, H. Takagi, Science **328**, 474 (2010).
 - ⁴² M. P. Allan *et al.*, Science **336**, 563 (2012).
 - ⁴³ A. Miura *et al.*, Mat. Res. Exp. **1**, 016002 (2014).